ARTICLE

Enhancement of device performance of organic solar cells by an interfacial perylene derivative layer

Inho Kim,[†] Hanna M. Haverinen,[‡] Jian Li,[†] and Ghassan E. Jabbour*[,†,§]

School of Mechanical, Aerospace, Chemical and Materials Engineering and Advanced Photovoltaics Center, Arizona State University, 7700 South River Parkway, Tempe, Arizona 85284, and University of Oulu, P.O. Box 4500, 90014 Oulun Yliopisto, Finland

ABSTRACT We report that device performance of organic solar cells consisting of zinc phthalocyanine and fullerene (C_{60}) can be enhanced by insertion of a perylene derivative interfacial layer between fullerene and bathocuproine (BCP) exciton blocking layer (EBL). The morphology of the BCP is influenced by the underlying *N*,*N*′-dihexyl-perylene-3,4,9,10-bis(dicarboximide) (PTCDI-C6), which promotes migration of the cathode metal into the BCP layer. Insertion of a PTCDI-C6 layer between fullerene and BCP layers enhances the power conversion efficiency to 2.5%, an improvement of 32% over devices without PTCDI-C6 layer. The enhancement in device performance by insertion of PTCDI-C6 is attributed to a reduction in series resistance due to promoted metal migration into BCP and optimized optical interference effects in multilayered devices.

KEYWORDS: organic solar cells • exciton blocking layer • bathocuproine • perylene derivative

INTRODUCTION

Extensive research on organic solar cells has been carried out in order to further improve their performance since the first report of an efficient multilayered device based upon a metallophthalocyanine and a perylene derivative (1). In general, relatively high efficiency organic solar cells using small molecular weight organic materials have adopted the use of an optically transparent exciton blocking layer (EBL) between the cathode and acceptor (2). This layer has been reported to play multiple roles in multilayered organic solar cells based on small molecules (3). The EBL is thought to prevent diffusion of cathode metals such as Al and Ag into active organic layers during cathode metal deposition and consequently reduce electrical shorting and quenching of excitons. Optically transparent EBL layers can also work as optical spacers, i.e., the optical field intensity distribution of incident electromagnetic wave can be adjusted by varying the thickness of EBL. Thus, optimization of EBL thickness can lead to enhancement of optical absorption in organic active layers.

Bathocuproine (BCP) is one of the most widely used EBL materials because of its high transparency in the visible range. In addition to aforementioned effects, BCP also helps in ohmic contact formation between cathode metal (Al and Ag) and fullerene (C_{60}) (3). Charge carrier transport in BCP can be further assisted by gap states which are induced by metal migration into BCP during cathode metal deposition. Such gap states have been recently verified using photoelectron spectroscopic approach (4). A low-resistivity ohmic contact between the electrode and organic semiconductor is essential to achieve efficient charge extraction. The damage depth in organic semiconductors, where the gap states are generated, is determined by the atomic size of a metal element and its ionization energy (5). For Ag, the damage depth in BCP has been reported to be around 10 nm (6). To reduce the formation of electrical shorts, a BCP layer with thickness larger than 10 nm is normally used in most organic solar cells. However, increasing the thickness of the BCP layer causes carrier extraction difficulty, thus resulting in poor fill factor and low photocurrent because of the limited cathode metal damage depth in thicker BCP. Doping with an alkali metal such as Li has been reported to increase the conductivity of BCP significantly, and provides a scheme to reduce device series resistance (7). It is worth noting that gap states are not necessary for efficient operation of organic solar cells. In this regard, alternative materials, such as tris(acetylacetonato)ruthenium(III), exhibiting high mobility and good energy alignment with the cathode, have been reported as a promising EBL (8).

In this work, we propose an approach that extends the metal damage depth through inducing surface roughness in the BCP film due to the insertion of an interfacial layer between the acceptor and BCP. The material used for this purpose is a perylene diimide derivative with hexyl chains on both ends. This strategy enables organic solar cells to exhibit higher device performance than cells without the

* Corresponding author. E-mail: : jabbour@asu.edu or Ghassan.jabbour@kaust.edu.sa. Current address: Solar and Alternative Energy Engineering Research Center, Physical Science and Engineering, KAUST, Thuwal, Saudi Arabia.

Received for review January 15, 2010 and accepted April 09, 2010

† School of Mechanical, Aerospace, Chemical and Materials Engineering, Arizona State University.

‡ University of Oulu.

§ Advanced Photovoltaics Center, Arizona State University.

DOI: 10.1021/am100039m

Published on Web 04/21/2010

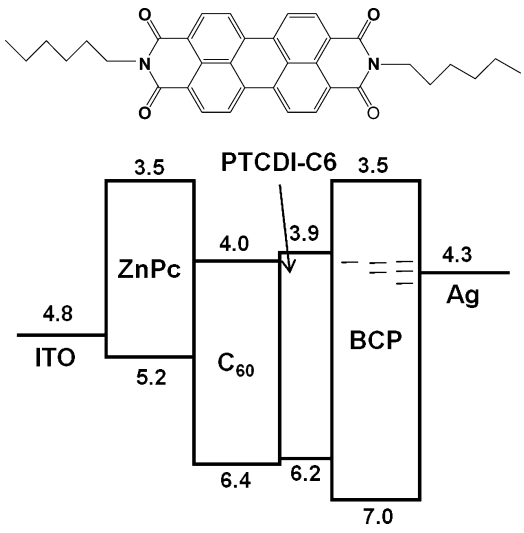

FIGURE 1. Molecular structure of PTCDI-C6 (top), and energy level diagram of devices having an interfacial layer of PTCDI-C6 (bottom). All energy levels are in eV.

interfacial layer. The effect of variation in BCP thickness on photocurrent is also discussed.

EXPERIMENTAL SECTION

Prior to device fabrication, patterned ITO substrates (Thin Film Device Inc.) were sonicated in common solvents before being exposed to plasma ashing for 5 min. Zinc phthalocyanine (ZnPc) and PTCDI-C6 were synthesized according to previously published literature (9, 10). C_{60} (99.9%) and BCP were purchased from MER Inc. (Tucson, AZ) and Alfa Aesar, respectively. All organic materials were purified using a four-temperature zone purifier. Devices were fabricated by successive thermal deposition of organic materials, followed by masked deposition of metal Ag cathode on patterned ITO glass substrates. Deposition rates of 0.5−1.0 Å/s were used at a working pressure of 1×10^{-7} Torr. ZnPc (25 nm) was used as the donor layer, and C_{60} (30 nm) was used as the acceptor layer. This was followed by the deposition of BCP with a varying thickness between 5 to 30 nm. To complete the device, a 100 nm Ag cathode was used. The active device area was 0.20 cm^2. Another set of devices was fabricated by insertion of a 5 nm PTCDI-C6 layer between the C_{60} and BCP layers.

Current−voltage characteristics were measured at room temperature in the dark, and under a solar simulator (Spectra Physics, Oriel 300W) with an AM1.5G filter at a light intensity of 100 mW/cm^2. The light intensity was adjusted with a Si reference cell which was calibrated by the National Renewable Energy Laboratory (NREL). EQE (external quantum efficiency) was measured with monochromatic light by varying the excitation wavelength from 400 to 800 nm at intervals of 10 nm, under a white bias light of 100 mW/cm^2. Surface morphology was measured using atomic force microscopy (AFM) (Veeco Dimension 3100) in tapping mode. The LUMO level of PTCDI-C6 in dimethylformamide was obtained from the reduction potential measured using cyclic voltammetry (CH Instrument, CHI600C) with an internal reference of ferrocene. The HOMO level of PTCDI-C6 was estimated by adding its optical gap energy from the LUMO level. An optical gap energy of 2.3 eV is obtained from the overlap between the optical absorption and photoluminescence spectra. In order to investigate metal diffusion into the organic layers, Rutherford back scattering (RBS) spectra were carried on two structures: Si/C_{60} (30 nm)/BCP (30 nm)/Ag (100 nm) and Si/C_{60} (30 nm)/PTCDI-C6 (5 nm)/BCP (30 nm)/Ag (100 nm). He^{2+} ions (2 MeV) were incident on the samples and the energies of backscattered particles were analyzed using a multichannel analyzer. To understand how surface energy affects the growth of BCP, we measured water contact angles for 70 nm-thickness BCP, C_{60} and PTCDI-C6 on glass (Krüss EasyDrop FM40). Optical refractive indices of organic materials used in optical modeling were determined by spectroscopic ellipsometry (J.A. Woollam M-2000).

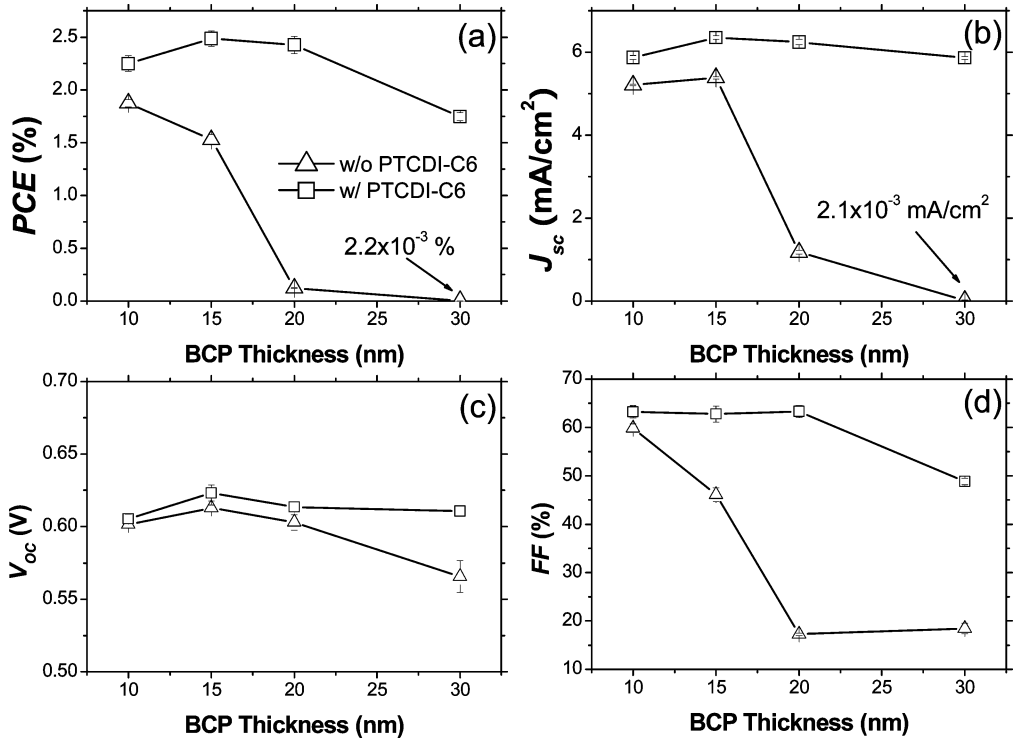

FIGURE 2. Device parameters for the cells with insertion of PTCDI-C6 between C_{60} and BCP (square), and without PTCDI-C6 (triangle): (a) PCE, (b) J_{sc}, (c) V_{oc}, and (d) FF.

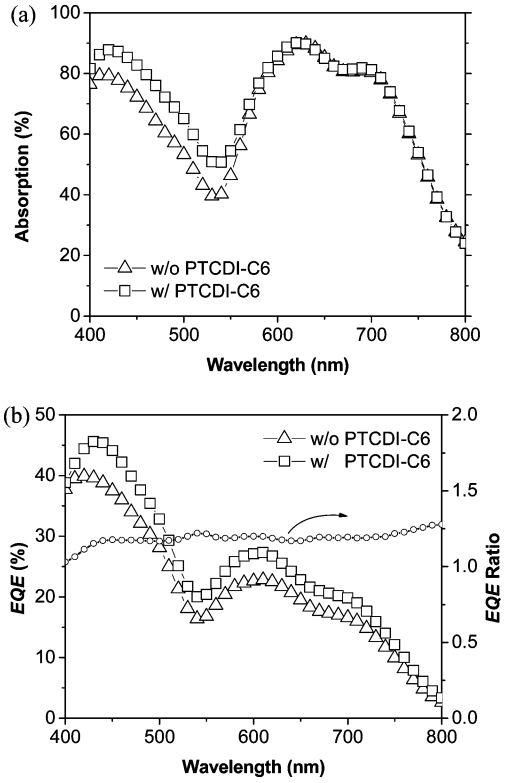

FIGURE 3. (a) Optical absorption of devices measured in reflection mode for cells with PTCDI-C6 (square), and without PTCDI-C6 (triangle). (b) EQE results for cells with PTCDI-C6 (square) and without PTCDI-C6 (triangle), and EQE ratio of both cells (open circle).

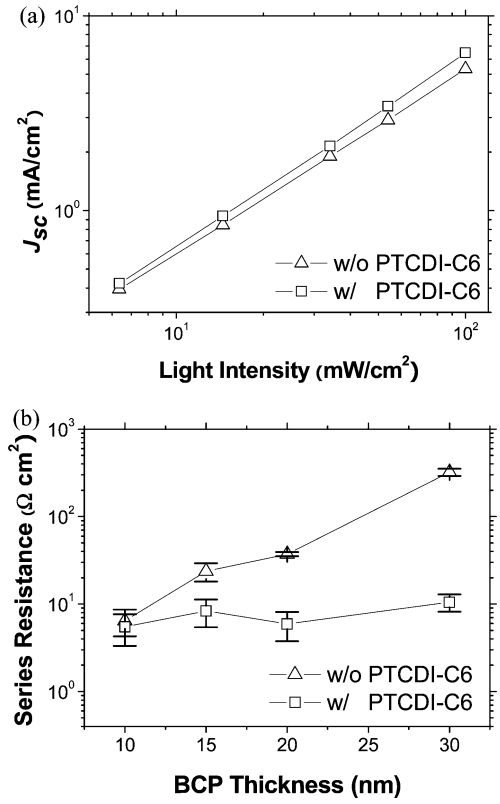

FIGURE 4. (a) J_{sc} vs light intensity and (b) specific series resistance vs BCP thickness for cells with PTCDI-C6 (square) and without PTCDI-C6 (triangle).

RESULTS AND DISCUSSION

Figure 1 shows the molecular structure of PTCDI-C6 and energy level diagram of the device structure used in this study. PTCDI with alkyl chains has been reported to be a good n-type material with high mobility and promising acceptor in organic solar cells (11, 12). The energy levels for all materials are extracted from literature except those of PTCDI-C6 (13). The HOMO and the LUMO energy levels of PTCDI-C6 were measured to be 6.2 and 3.9 eV, respectively. The LUMO level of PTCDI-C6 aligns well with the LUMO level of C_{60}, resulting in negligible energy barrier for charge transport between the two materials. The dashed lines within the BCP gap represent gap states induced by cathode metal deposition.

Device performance of zinc phthalocyanine (ZnPc)/C_{60} solar cells with and without the interfacial PTCDI-C6 layer, and with various BCP thicknesses from 10 to 30 nm, is shown in Figure 2a–d. Device structures used are as follows: ITO/ZnPc (25 nm)/C_{60} (30 nm)/PTCDI-C6 (0 or 5 nm) /BCP (5–30 nm)/Ag (100 nm). Devices having 5 nm of BCP failed because of a large leakage current, and thus not shown. For cells without the PTCDI-C6 layer, the power conversion efficiency (PCE) decreases drastically from 1.9 to 0.002% while increasing BCP thickness from 10 to 30 nm. This is ascribed to a rapid decrease in short circuit current density (J_{sc}) and fill factor (FF). In contrast, cells with PTCDI-C6 show an overall superior performance. In this case, increasing the thickness of the BCP layer results in increased *PCE* and J_{sc}. Peak performance values at 15 nm followed by a slight decrease at 20 nm are observed, which appear to be due to optical interference effects in multilayered devices, which will be discussed later in this paper. Cells with device structure of ZnPc/C_{60}/PTCDI-C6/BCP (15 nm)/Ag showed a high PCE of 2.5%, a 32% improvement over devices without PTCDI-C6.

The interfacial layer of PTCDI-C6 has a broad optical absorption at wavelength of 400–600 nm and is a good acceptor material for organic solar cells (14). Figure 3a shows optical absorption and EQE for devices with and without PTCDI-C6, each having 15 nm BCP layer. The optical absorption was measured in reflection mode, where absorption was obtained by measuring the reflection and subtracting it from 100%. Figure 3a indicates more absorption in devices with PTCDI-C6 at wavelengths of 400–600 nm compared to devices without PTCDI-C6 layer. As described above, the enhancement in PCE values with a PTCDI-C6 layer is a consequence of improved J_{sc} value, which is confirmed by the EQE measurement. As shown in Figure 3b, the EQE for devices with PTCDI-C6 intermediate layer is higher than that of devices without PTCDI-C6, at 400 nm –800 nm range. However, the ratio of EQE values in this wavelength range for both devices is constant (~1.2), indicating no characteristic contribution to the photocurrent from PTCDI-C6.

Additionally, J_{sc} for cells with 15 nm BCP were measured with varying light intensity from 0.06 to 1 sun, as shown in Figure 4a. The slope of J_{sc} vs light intensity in log–log scale indicates the efficiency of carriers extraction through the electrodes. A slope less than unity implies that photocurrent

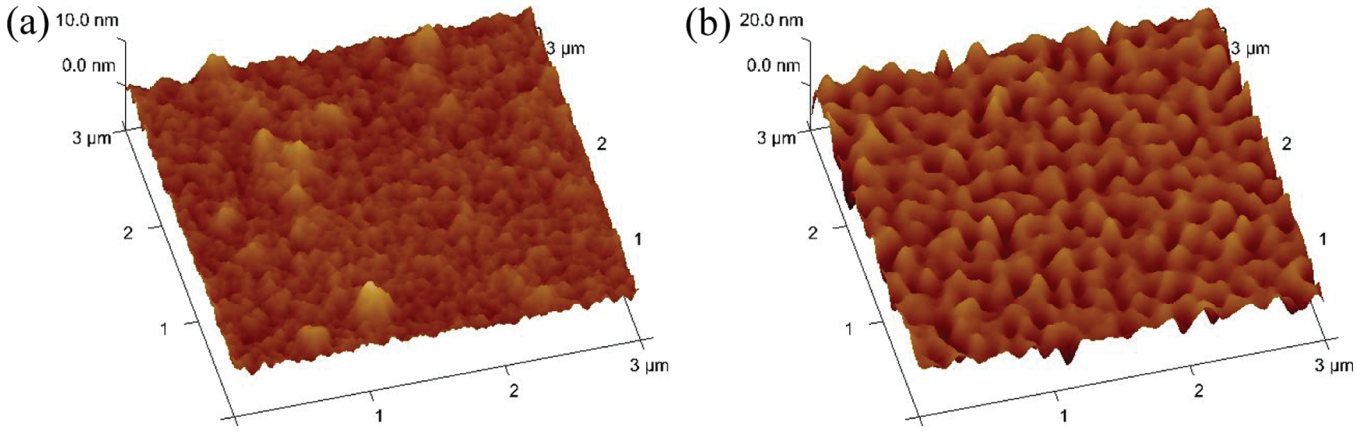

FIGURE 5. AFM height image for organic layers on glass substrates: (a) C_{60} (30 nm)/ BCP (15 nm) and (b) C_{60} (30 nm)/PTCDI-C6 (5 nm)/BCP (15 nm).

is limited by electron−hole pair recombination attributed to space charge effect or series resistance (15). The slope for both cells with and without PTCDI-C6, obtained by least-squares fitting method, is 1.00 and 0.96, respectively. Figure 4b shows the series resistance of the cells as a function of BCP thickness. The series resistance of devices without the interfacial layer increases abruptly with increasing BCP thickness, while the insertion of PTCDI-C6 leads to negligible increase in the series resistance. These findings suggest that the insertion of PTCDI-C6 reduces the contact resistance in C_{60}/BCP, resulting in an enhancement of J_{sc} through reduction in electron−hole pair recombination at a donor/acceptor interface.

To understand the origin of the reduction in series resistance with insertion of PTCDI-C6, the surface morphologies of BCP thin films on C_{60} and PTCDI-C6 were investigated using an atomic force microcopy (AFM). Images a and b in Figure 5 show the dependence of BCP topography upon different underlying organic layers of glass/C_{60} and glass/C_{60}/PTCDI-C6 respectively. BCP film deposited on glass/C_{60} (30 nm) has an rms roughness of 0.8 nm and peak-to-valley height of 8.8 nm. In contrast, the BCP film on glass/C_{60} (30 nm)/PTCDI-C6 (5 nm) exhibits a noticeably rougher surface with rms roughness and peak-to-valley height values of 2.6 and 22 nm, respectively. These results point to the influence of the underlying PTCDI-C6 on the morphology of the BCP layer. The contact angle values of water on C_{60}, PTCDI-C6 and BCP thin films were 75°, 92° and 64°, respectively. The lower contact angle of the BCP thin film indicates their hydrophilic characteristics when compared with PTCDI-C6. The hydrophobic nature of PTCDI-C6 layer may affect the growth of hydrophilic BCP, leading to a rougher surface than that of BCP grown directly on hydrophilic C_{60}. This roughness in turn may enhance metal migration into BCP, which reduces series resistances in devices because of an increase in the BCP conductivity, as described before. The reduced resistance leads to improved charge collection efficiency as demonstrated by the measurement of J_{sc} vs illumination intensity (Figure 4a).

To obtain a direct evidence of metal diffusion into BCP, Rutherford backscattering spectroscopy (RBS) was carried out on two samples: (a) Si/C_{60} (30 nm)/BCP (30 nm)/Ag (100 nm) and (b) Si/C_{60} (30 nm)/PTCDI-C6 (5 nm)/BCP (30 nm)/Ag (100 nm). The results are shown in Figure 6. There is a strong peak around channel of 300, which originates from Ag. The slight shift, around channel 275, to low energy of the RBS spectra for sample b indicates a migration of Ag into the BCP layers to a depth of up to 15 nm compared to sample a.

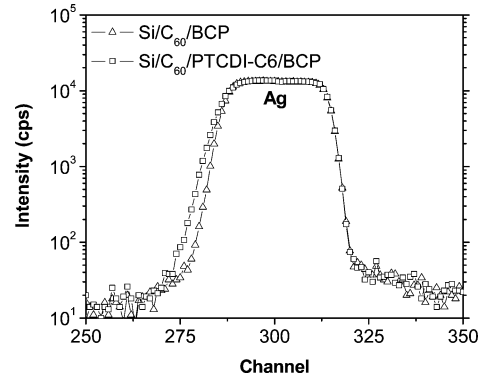

FIGURE 6. RBS spectra for (a) Si/C_{60} (30 nm)/BCP (30 nm)/Ag (100 nm) and (b) Si/C_{60} (30 nm)/PTCDI-C6 (5 nm)/BCP (30 nm)/Ag (100 nm).

The slight variation in J_{sc} vs BCP thickness for cells with PTCDI-C6 observed in Figure 2 can be understood by considering optical interference effects in a multilayered device structure. As shown in Figure 2b, the highest J_{sc} was achieved with a BCP thickness of 15 nm. The maximum optical field intensity should be located at donor/acceptor interface for photons to be harnessed efficiently in planar heterojunction solar cells because PCE is primarily limited by exciton diffusion. To investigate further the interference effects due to varying the BCP thickness, we carried out optical modeling using a transfer matrix algorithm (16). Figure 7a shows the calculated optical field distribution in ITO/ZnPc/C_{60}/PTCDI-C6/BCP/Ag devices with varying BCP thickness of 0, 5, 10, 15, 20, and 25 nm at incident light wavelength of 610 nm. The maximum optical field intensity lies at approximately $\lambda/4n$ from the metal cathode, where λ is the wavelength of incident light and n is the refractive index of organic materials. As the thickness of BCP increases, the optical field peak position shifts toward the cathode. At 15 nm of BCP thickness, the peak position is

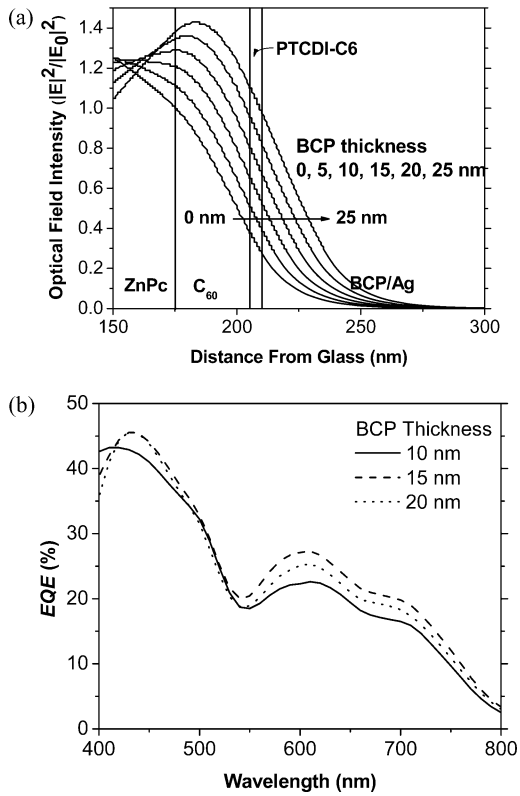

FIGURE 7. (a) Calculated optical field distribution at wavelength of 610 nm for devices having the structure of ITO/ZnPc (25 nm)/C_{60} (30 nm)/PTCDI-C6 (5 nm)/BCP (0−30 nm)/Ag (100 nm). Optical field intensity ($|E|^2$) is normalized with incident light intensity ($|E_0|^2$). (b) Measured EQE of cells with BCP thickness of 10 nm (solid line), 15 nm (dashed), and 20 nm (dotted).

located approximately at the donor−acceptor interface, and as it becomes thicker, the peak position moves beyond this interface toward the cathode, which would reduce photocurrent contribution from ZnPc. Similarly, at a wavelength of 420 nm, the optical field peak shifts toward the cathode. Figure 7b shows the measured EQE for cells with BCP thickness of 10, 15, and 20 nm. The comparison of EQE values indicates that the highest J_{sc} from cells with 15 nm BCP is due to enhanced EQE around 600 nm, which is mainly contributed by ZnPc. For cells with 20 nm of BCP, the EQE decreases at wavelength of 600 nm, which is well-explained by the optical field distribution in Figure 7a. In contrast, the EQE value at a wavelength of 400−500 nm is less sensitive to the optical field distribution, which is possibly due to longer exciton diffusion length of C_{60} (~40 nm) than ZnPc (~10 nm) (17).

CONCLUSION

In summary, we have demonstrated that the insertion of a PTCDI-C6 layer between C_{60} and BCP layers in a solar cell structure based on ZnPc and C_{60} enhances PCE from 1.9 to 2.5%. The interfacial layer (PTCDI-C6) roughness affects the growth of BCP, which promotes the migration of Ag deeper into the BCP layer, thus enhancing the charge collection at the cathode. This extension of the bandgap states through enhancing the damage depth in BCP was confirmed with RBS spectroscopy measurement. Moreover, insertion of a PTCDI-C6 layer makes it possible to utilize thicker BCP without substantial increase in series resistance. This approach also provides the possibility of taking advantage of optical interference effects through an adjustment of the BCP thickness.

Acknowledgment. The authors acknowledge useful discussions with Dr. Parul Dhagat, Dr. Madhusudan Singh, and Dr. Xiaohui Yang, and thank the Advanced Photovoltaics Center and the National Science Foundation for the partial support of this work (CBET-0756148). H.M.H and G.E.J. also acknowledge the Graduate School of Modern Optics and Photonics and the FiDiPro of Finland for their support.

REFERENCES AND NOTES

(1) Tang, C. W. *Appl. Phys. Lett.* **1986**, *48* (2), 183.
(2) Peumans, P.; Forrest, S. R. *Appl. Phys. Lett.* **2001**, *79* (1), .
(3) Vogel, M.; Doka, S.; Breyer, C.; Lux-Steiner, M. C.; Fostiropoulos, K. *Appl. Phys. Lett.* **2006**, *89*, 163501.
(4) Takeaki, S.; Susumu, T.; Hikaru, K.; Shigeru, M.; Hiroo, K.; Katsuhiro, A. *J. Appl. Phys.* **2010**, *107* (4), 043707.
(5) Hirose, Y.; Kahn, A.; Aristov, V.; Soukiassian, P. *Appl. Phys. Lett.* **1996**, *68* (2), 217–219.
(6) Peumans, P.; Yakimov, A.; Forrest, S. R. *J. Appl. Phys.* **2003**, *93* (7), 3693.
(7) Parthasarathy, G.; Shen, C.; Kahn, A.; Forrest, S. R. *J. Appl. Phys.* **2001**, *89* (9), 4986–4992.
(8) Rand, B. P.; Li, J.; Xue, J.; Holmes, R. J.; Thompson, M. E.; Forrest, S. R. *Adv. Mater.* **2005**, *17*, 2714.
(9) Würthner, F. *Chem. Commun.* **2004**, (14), 1564–1579.
(10) Brown, R. J. C.; Kucernak, A. R.; Long, N. J.; Mongay-Batalla, C. *New J. Chem.* **2004**, *28* (6), 676.
(11) Chesterfield, R. J.; McKeen, J. C.; Newman, C. R.; Ewbank, P. C.; Filho, D. A. d. S.; Bredas, J.-L.; Miller, L. L.; Mann, K. R.; Frisbie, C. D. *J. Phys. Chem. B* **2004**, *108*, 19281.
(12) Pandey, A. K.; Dabos-Seignon, S.; Nunzi, J.-M. *Appl. Phys. Lett.* **2006**, *89*, 113506.
(13) Falkenberg, C.; Uhrich, C.; Olthof, S.; Maennig, B.; Moritz, K. Riede; Leo, K. *J. Appl. Phys.* **2008**, *104*, 034506.
(14) Kim, I.; Haverinen, H. M.; Wang, Z.; Madakuni, S.; Li, J.; Jabbour, G. E. *Appl. Phys. Lett.* **2009**, *95*, 023305.
(15) Mihailetchi, V. D.; Wildeman, J.; Blom, P. W. M. *Phys. Rev. Lett.* **2005**, *94*, 126602.
(16) Pettersson, L. A. A.; Roman, L. S.; Inganäs, O. *J. Appl. Phys.* **1999**, *86* (1), 487.
(17) Rand, B. P.; Genoe, J.; Heremans, P.; Poortmans, J. *Prog. Photovoltaics: Res. Appl.* **2007**, *15*, 659.

AM100039M